Friction **6**(1): 84–97 (2018)
https://doi.org/10.1007/s40544-017-0167-5
ISSN 2223-7690
CN 10-1237/TH
RESEARCH ARTICLE

Chemical effects on the sliding friction of Ag and Au(111)

H. E. KO, S. G. KWAN, H. W. PARK, A. CARON*
KoreaTech–Korea University of Technology and Education, Chungnam Province 330-708, Republic of Korea
Received: 08 February 2017 / Revised: 22 April 2017 / Accepted: 10 May 2017

Abstract: We have investigated the sliding friction behavior of metallic couples with different enthalpy of mixing or reaction by friction force microscopy. Comparing the friction behavior of miscible and immiscible couples we find that in the first case friction is governed by adhesion while the shear strength is low (τ = 3–6 MPa). In the latter case of immiscible couples, adhesion is found to be low and the shear strength is large ($\tau \approx 70$ MPa). Statistical analysis of atomic stick-slip images recorded on an Au(111) surface with tips of different affinities with gold allows for a deeper understanding of our results. The periodicity of atomic stick-slip images corresponds to the interatomic distance of gold for immiscible counter-bodies. In contrast, for a reactive couple the periodicity of atomic stick-slip significantly differs from the gold interatomic distance and may correspond to the structural length of an ordered intermediate phase at the tip-surface interface.

Keywords: metals; surface; friction; nanotribology; atomic force microscopy

1 Introduction

Understanding and controlling the friction between materials is crucial for the development of new devices. With the development of atomic force microscopy (AFM) and friction force microscopy (FFM), the sliding response of a nanometer-scaled single asperity onto flat surfaces has become experimentally accessible. This has allowed bridging the gap between macro-scale measurements of friction and wear and their underlying theories based on mechanisms taking place at the microscopic scales. Owing to their technical relevance, the studies of friction and wear have long been focused on metals. The friction and wear of metals has been described in terms of two main mechanisms (see for example Refs. [1, 2]):

- The formation and shearing of adhesive bonds between surface asperities leading ultimately to their rupture and material transfer;
- The ploughing of a softer surface by a harder asperity involving plastic deformation and debris formation.

The development of nano-/micro-fabrication methods has given raise to the production of nano-/micro-electromechanical devices (N/MEMS) [3]. Such devices are usually based on silicon. For such application the use of liquid lubricant is not possible. Oxidized silicon surfaces have been known to have poor tribological properties [4]. The growth of thin metallic films onto silicon devices for operation in reciproc motion appears to be a feasible alternative. Recently, the nanoscale friction and wear behavior of metals has been investigated [5–10]. In the low load regime where adhesive force prevails, friction has been reported to vanish and the sliding of a slingle asperity onto single crystalline metallic surfaces was characterized by atomic stick-slip [5]. Further the effect of surface modifications on the nanotribology of Au(111) has been investigated and compared to the nanotribological response of a clean Au(111) surface [7]. There the author demonstrated the role of a Au-neck formation at the AFM-tip/Au(111) interface on the nanotribology of gold. Further, the authors demonstrated the role of passivating self-assembled monolayer in suppressing the formation

* Corresponding author: A. CARON, E-mail: arnaud.caron@koreatech.ac.kr

of such a neck and the switching of nanoscale friction on Au(111) by electrochemical control. Moreover, the nanotribology of thermanlly deposited gold on graphite was studied [8, 9]. In contrast to single-asperity friction measurements performed in ultra-high vacuum (UHV)-conditions in Refs. [5, 6], the authors reported on $F_n^{2/3}$-dependence of the friction force on gold nano-particles measured in ambient conditions, where F_n is the normal force [8]. In Ref. [9] the sliding of gold nano-island deposited on graphite was reported to yield similar friction values as in UHV-conditions, thus pointing at the importance of chemical inertness of the tribological couple and the abesence of contamination at the sliding interface for superlubricity. The effect of tip chemistry has been inferred as the coefficients of friction measured on Pt(111) with a SiO_x AFM-tip or a diamond AFM-tip differed by an order of magnitude [10]. At larger load wear was observed to be mediated by mechanisms of plastic deformation [10].

In this work we investigate the sliding friction behavior of different metallic couples with different enthalpies of mixing or reaction by means of FFM. We discuss our results on the basis of the adhesive friction theory of metals. Further, we perform statistical analysis of the observed atomic stick-slip on Au(111) with tips of different chemistries to provide new insights in the surface reactivity of metallic couples.

2 Samples preparation and characterization

A polycrystalline high purity Ag sample purchased from Alfa Aesar was metallographically prepared by mechanical grinding with SiC paper and polishing with diamond suspension with a particle size down to 1 μm. Subsequently, vibration polishing with a Al_2O_3 suspension with a particle of 25 nm was applied. A 200 nm thick polycrystalline Au(111) layer grown by physical vapor deposition on mica was purchased by Phasis, Switzerland.

Figure 1 shows (a, d, e) non-contact and (b, c) contact AFM topography images recorded on the as-prepared Ag sample and the as received Au sample. The non-contact AFM images were recorded with a stiff diamond coated cantilever (type: CDT-NCLR, manufactured by NanoSensors, Switzerland) with a first bending resonance frequency f_0 = 192.54 kHz and a bending stiffness C_n = 50.14 N/m. The contact AFM images were recorded with a soft PtSi coated cantilever (type: PtSi-CONTR, manufactured by NanoSensors, Switzerland) with a first bending resonance frequency f_0 = 14.05 kHz and a bending stiffness C_n = 0.386 N/m. The topography images of the metallographically prepared Ag surface reveal its polycrystalline microstructure. The polycrystalline nature of the Au thin film grown on mica is evidenced in the topography image shown in Fig. 1(d). Higher magnification images

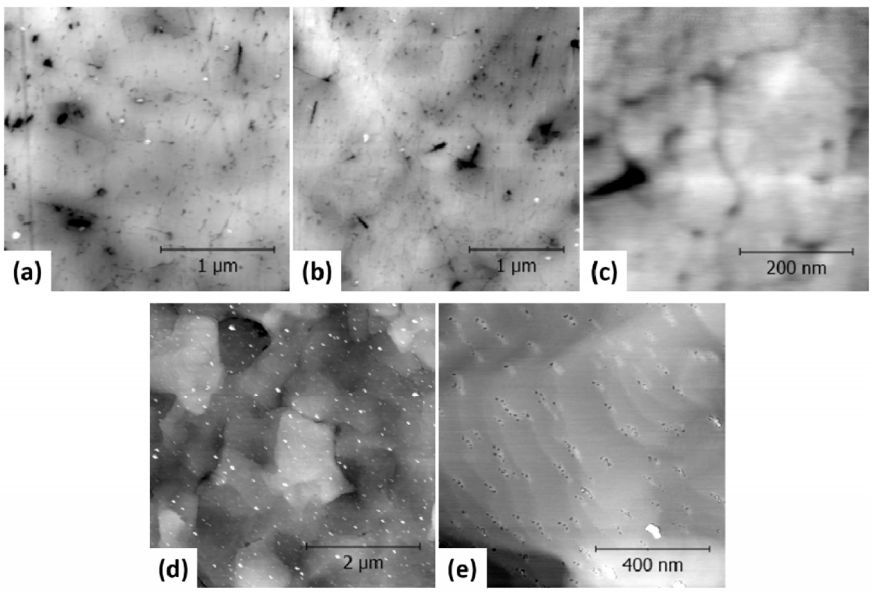

Fig. 1 AFM-topography images on (a–c) polycrystalline Ag and (d, e) a polycrystalline Au(111) thin film grown on mica.

within a single grain show atomically smooth terraces with a width of the order of 100 nm and atomic steps with heights of 0.288 nm or multiples (see Fig. 1(e)). Also to be observed on the topography images recorded on Au(111) is the presence of adsorbates concentrated at steps.

3 Experimental methods

Sliding friction experiments were performed in ambient conditions (T = 293 K, RH = 40%) by FFM [11] using an AFM XE-100 manufactured by Park Instruments, Rebuplic of Korea, with three different soft AFM-cantilevers of the types PtSi-CONTR, CONTSC-Au and CONTSC-Pt (manufactured by NanoSensors, Switzerland) for each samples. A single tip of each type and for each sample has been used for repeated measurements. The authors would like to stress out the representative character of the measurements presented here. The significance of AFM-measurements relies on the idealization of a tribological contact between a smooth surface and a single asperity, i.e., the AFM-tip. As demonstrated in Fig. 2 the geometry of the different tip apex could be treated as equivalent. The chemistry of the counter bodies was chosen on the basis of the respective phase diagrams between the samples and counter bodies, in order to probe the effect of miscibillity between tip and sample materials. Owing to its chemical inertness and its high thermodynamic stability a PtSi counter body was used as a reference and in order to realize the case of complete immiscibility with Ag and Au(111). The thermodynamic stability of PtSi is demonstrated by its high melting point T_m = 1,504.74 K [12] and its highly negative standard enthalpy of formation ΔH_f = −118 kJ/mol [13]. In contrast, a gold counter body was selected owing to its full miscibillity with Ag so as to exemplify the case of a negative enthalpy of mixing (ΔH^{mix}_{Au-Ag} = −4.5 kJ/(g·atom) at 800 K) [14], on the one hand. On the other hand, the case of a Au counter body sliding on a Au(111) surface serves the purpose of realizing a tribological couple with a zero enthalpy of mixing. Moreover, a platinum counter body was selected to study the effect of imiscibillity between materials involved in a tribological couple; the Ag–Pt phase diagram exhibits a peritectic decomposition of the liquid phase characterized by a peritectic temperature of 1,459 K and a peritectic concentration X_{Pt} = 40.6 at.%. At room temperature a biphased domain is usually accepted although the existence of intermetallic phases below 1,238 K is still under debat (see Ref. [14]). Further, the Au–Pt phase diagram exhibits a miscibillity gap below 1,533 K at X_{Pt} = 61 at.%. At room temperature Pt is soluble into Au up to X_{Pt} = 7 at.%; for larger platinum compositions the Au–Pt phase diagram exhibits a biphased domain at room temperature [14].

Prior to friction experiments and for each cantilever used in this work the sensitivity of the AFM-photodiode S was calibrated by recording a force distance curve on the respective sample surfaces and by calculating the slope of the repulsive part of the curve. Subsequently, the bending and torsion stiffness

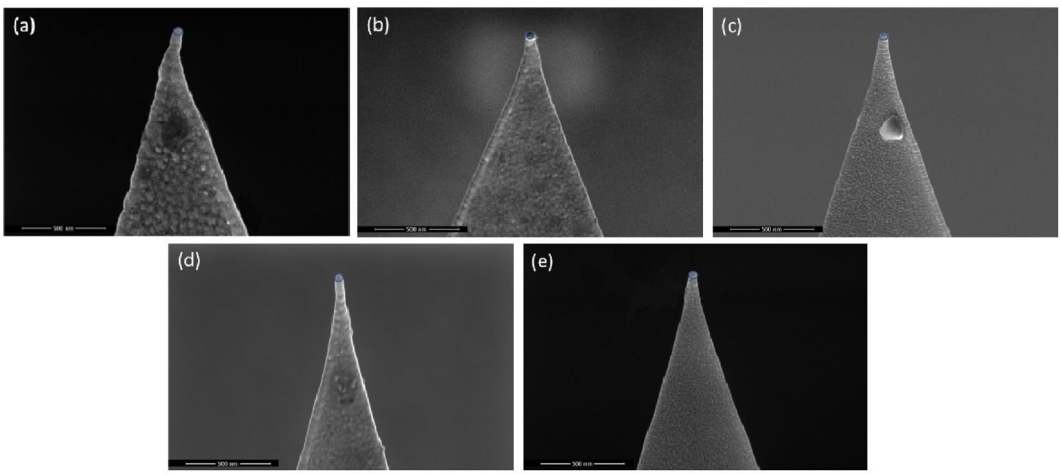

Fig. 2 SEM images of the AFM tips used for friction measurements on (a–c) Ag and (a, d, e) Au(111): (a) PtSi-coated tip, (b, d) Au-coated tips, (c, e) Pt-coated tips.

of each cantilever were determined from its thermal noise vibration [15]. The cantilevers' stiffnesses are listed in Table 1. The friction experiments consisted in recording the lateral deflection signal of the AFM-cantilevers in both forward and backward direction of the *x*-scanner. Thereby the lateral deflection signal V_l was recorded in volt and was subsequently converted into units of force according to $F_L = \frac{3}{2} C_l \frac{h}{L} S V_l$ [16], where h, the tip height, was taken to be 12 μm, in agreement with the manufacturer's data. In the case of Ag the images size was selected as 500 nm × 500 nm and experiments were recorded with a normal load F_n = 0–10 nN. In the case of Au(111) the experiments were performed over an area of 10 nm × 10 nm with a normal load F_n = 0–10 nN. On Au(111) friction measurements were repeated twice for each load value. In this work, two different scan areas were selected for Ag and Au(111). On the polished Ag surface a larger scan area was selected to average out the effects of topography resulting from the surface preparation. With such a preparation method of the Ag sample no atomically smooth surface can be achieved. The as-sputtered Au(111) thin film on mica displayed large atomically flat terraces that were suitable to perform friction measurements at the atomic scale. While the measurements on Ag aimed at a proof of concept, we expected the measurements on Au(111) to further provide insights into the mechanisms responsible for the chemical effects on metals friction at the atomic scale.

For each measurement the friciton force was calculated according to $F_f = \frac{F_{L,fwd} - F_{L,bwd}}{2}$, where $F_{L,fwd}$ and $F_{L,bwd}$ are the forward and backward images of the lateral force, respectively. Subsequently, the calculated friction force image was averaged line-by-line and a corresponding error was calculated as the standard deviation from the mean value using the Matlab software package (see script1.m in Electronic Supplementary Material (ESM)) [17]. Moreover the shear strength τ and the adhesion force F_{ad} corresponding to each tribological couple were calculated by fitting the $F_f(F_n)$-plot with the function $F_f = \tau A_c(F_n)$, where we consider τ to be a constant and $A_c(F_n)$ is the normal force dependent real area of contact between surface and tip (see Refs. [18]). In the frame of the Hertzian theory of elastic contact between a spherical body and a flat surface the real contact area is expressed as $A_c = \pi \left[\frac{3}{4} \frac{F_n R}{E^*} \right]^{2/3}$, where R is the radius of the spherical body and $E^* = \left[\frac{1-\nu_1^2}{E_1} + \frac{1-\nu_2^2}{E_2} \right]^{-1}$ is the reduced modulus of elasticity, and E_i and ν_i are the Young's moduli and the Poission's radii of the two elastic bodies involved in the contact [19]. The Hertzian contact theory however do not consider the effect of adhesion forces. Based on the Johnson-Kendall-Roberts (JKR) theory the real area of an adhesive contact between a spherical elastic body and the flat surface of an elastic body can be expressed as $A_c = \pi \left(\frac{R}{E^*} \right)^{2/3} \left[(F_n - F_{ad}) + 2F_{ad} + \sqrt{4F_{ad}(F_n - F_{ad}) + (2F_{ad})^2} \right]^{2/3}$, where F_{ad} is the adhesion force between the two elastic bodies [19]. Inserting this expression of A_c into $F_f = \tau A_c(F_n)$ results in a $F_n^{2/3}$-dependence of the friction force that has for expemple been experimentally observed in Refs. [8, 18, 20]. Following values were used for the Young's modulus and the Poisson's ratio: E_{Ag} = 83 GPa and ν_{Ag} = 0.37, E_{Au} = 75 GPa and ν_{Au} = 0.44, E_{Pt} = 168 GPA and ν_{Pt} = 0.38, and E_{PtSi} = 238.5 GPa

Table 1 Vertical and lateral stiffnesses, C_n and C_l, length L of the cantilevers and tip radius of curvature R (*manufacturer's data, **estimated data from SEM measurements).

Sample	Cantilever type	C_n (N/m)	C_l (N/m)	L^* (mm)	R^{**} (nm)
Ag and Au(111)	PtSi-CONTR	0.396	307.403	450	25
Ag	CONTSC-Au	0.650	129.21	225	25
Ag	CONTSC-Pt	0.783	155.71	225	25
Au(111)	CONTSC-Au	0.685	136.24	225	25
Au(111)	CONTSC-Pt	0.951	188.91	225	25

and ν_{PtSi} = 0.316 [21, 22]. In this work the radius of curature R was determined for each tip from scanning electron microscopy (SEM) images recorded after the friction experiments (see Fig. 2 and Table 1) using a Helios 600i dual-beam FIB-SEM manufactured by FEI, the Netherland. For all tips a similar value $R \approx 25$ nm was found and used to fit the experimental $F_f(F_n)$-plots. In Fig. 2(a) circle with a radius of 25 nm is overlaid on each of the tips to demonstrate the validity of this value. Furhter, elemental chemical analysis by energy dissipative X-ray spectroscopy (EDS) was performed in SEM at the apex of the Pt-tip shown in Fig. 2(e) after friction measurements on Au(111) by using a XFlash Detector 6 manufactured by Bruker, Germany.

In the case of Au(111) atomic-scale stick-slip was observed with all tips and statistically analyzed. A first analysis consisted in calculating the slip-length and its frequency as a function of the load. Thereby, the peak force positions in each line of recorded $F_{L,fwd}$-images were determined with the *findpeaks*-function of the Matlab software package [17]. Beforehand an average-baseline had been calculated and subtracted from each line of the image. To account for the instrumental noise, we also fitted our experimental data line-by-line with an interpolant function (*spline*-function). After determination of the peak force positions, the slip-distances were calculated as the distance between two successive force peaks for each line of the analyzed image and plotted in a single histogram (see script2.m in ESM). A second analysis consisted in line-by-line calculation of the power spectral density (PSD)-function of each recorded $F_{L,fwd}$-images using the *pburg*-function of the Matlab software package (see script3.m in ESM) [17]. The calculated PSD-functions corresponding to each line were averaged to provide a single PSD-function out of one $F_{L,fwd}$-image. This statistical analysis transforms a signal in real-space into a one-dimensional reciprocal space (k-space) signal, from which characteristic wavelengths $\lambda = 2\pi/k$ can be identified.

4 Results

Figure 3 shows the load dependence of friction on polycrystalline Ag and on Au(111) with three different counter-bodies: PtSi, Au, and Pt; the corresponding shear strength and adhesion force values are listed in Table 2. In the case of Ag, the load dependent friction force values were found lowest with a PtSi-coated tip. Fitting the load dependence of the friction for the Ag/PtSi tribological couple yields a shear strength value τ = 74.97 MPa and an adhesion force value F_{ad} = 5.26 nN. For the same sample, the largest load dependent friction force values were obtained with a Au-coated tip and corresponded to a shear strength

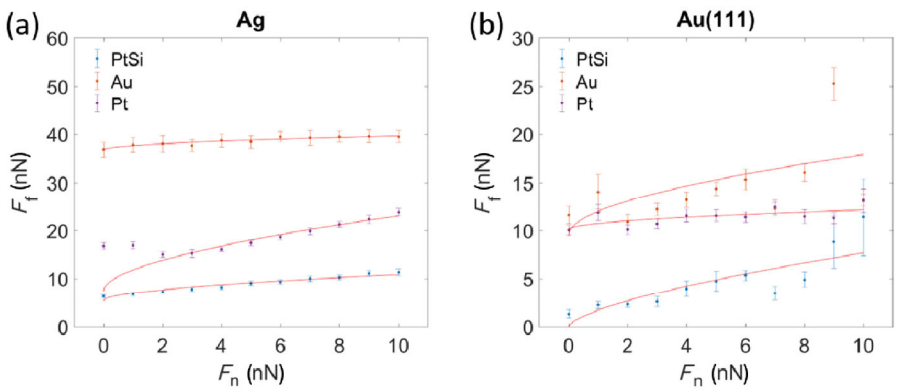

Fig. 3 Load dependence of friction on (a) polycrystalline Ag and (b) Au(111) with different counter bodies. In (a, b) the experimental data corresponding to the different tribological couples are fitted with a function of the type $F_f = \tau A_c(F_n)$, where τ is the shear strength and the real contact area A_c is expressed according to the JKR-model [18, 19]. Note that the fitting of the $F_f(F_n)$-plot corresponding to the Ag/Pt tribological couple excluded the data points corresponding to F_n = 0 nN and 1 nN. This exclusion is motivated by the assumption that a tip change occurs at the transition between F_n = 1 nN and 2 nN. For the Au(111)/Au tribological couple the data point corresponding to F_n = 10 nN was excluded from the fit, since this load correspond to the onset of wear, as evidenced by the disappearance of atomic stick-slip.

Table 2 Shear strength τ and adhesion force F_{ad} of the different tribological couples investigated in this work.

Sample	Counter body	τ (MPa)	F_{ad} (nN)
Ag	PtSi	74.97	5.26
	Au	3.7	2805
	Pt	24.41	19.07
Au(111)	PtSi	68.21	0
	Au	24.21	25.8
	Pt	6.6	443.5

τ = 3.7 MPa and an adhesion force F_{ad} = 2,805 nN. Both cases represent the extreme of fully-immiscible tribological partners in the case of Ag/PtSi and fully miscible partners in the case of Ag/Au. For the Ag/Pt tribological couple the load dependent friction force values were intermediate but closer to the values obtained with a Pt-coated tip than with an Au-coated tip. For the Ag/Pt tribological couple, we found τ = 24.41 MPa and F_{ad} = 19.07 nN. The Ag–Pt phase diagram exhibits a peritectic decomposition with a bi-phased domain over all compositions at room temperature, where Ag and Pt are thus immiscible.

In the case of Au(111), the load dependent friction force values was found to be highest with an Au-coated tip. For this tribological couple a shear strength value τ = 24.21 MPa and an adhesion force value F_{ad} = 25.8 nN were evaluated. The lowest value of the shear strength τ = 6.6 MPa and the largest adhesion force value F_{ad} = 443.5 nN were found for the Au/Pt tribological couple, whose load dependent friction force values are slightly lower than for the Au/Au tribological couple. The lowest load dependent friction force values were measured for the Au/PtSi tribological partner, for which τ = 68.21 MPa and F_{ad} = 0 nN were found. The lowest adhesion force and highest shear strength values correspond to the case of full immiscibility between PtSi and Au(111). On the opposite the largest adhesion force and lowest shear strength values correspond to the case of partial miscibility between Pt and Au(111). Pt has a large solubility in Au up to ~8 at.% at room temperature. For larger Pt-concentrations the Au-Pt phase diagram exhibits a miscibility gap. At small Pt-concentration the free Gibbs energy of mixing with Au is thus negative. For the Au/Au tribological couple, in which case the free Gibbs energy of mixing can be taken as zero, we found the load dependent friction force values to correspond to a shear strength τ = 24.21 MPa and an adhesion force F_{ad} = 25.8 nN.

Figure 4 shows three friction images and corresponding friction loops recorded on Au(111) with a PtSi-coated tip, a Au-coated tip and a Pt-coated tip. In all cases, atomic scale stick-slip can be observed.

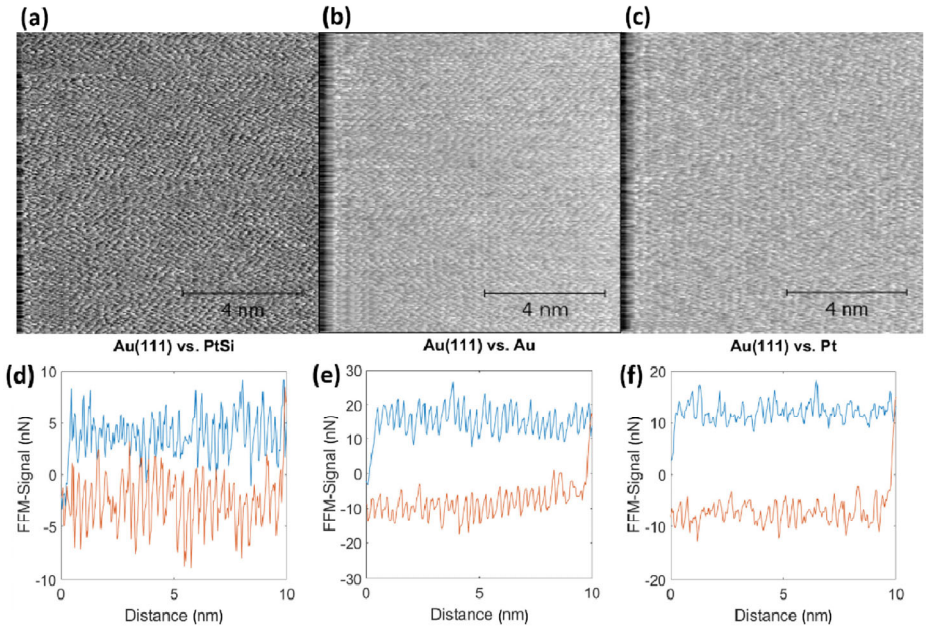

Fig. 4 (a–c) FFM images and corresponding (d–f) friction loops recorded on Au(111) with (a, d) a PtSi-coated tip, (b, e) an Au-coated tip, and (c, f) a Pt-coated tip.

From these measurements one can however recognize that the periodicity of the friction signal significantly depends on the tip chemistry, with the friction signals recorded with a PtSi-coated tip and an Au-coated tip appearing to be the more periodic than the signal recorded with a Pt-coated tip. In the case of the friction signal recorded with an Au-coated tip we further observe that the sticking force was almost constant. With a PtSi-coated tip sliding on Au(111), we observe a modulation of the sticking force. In the case of the Pt-coated tip the friction signal is less ordered. To compare the degree of order/disorder of the friction measurements performed with tips of different chemistries, we statistically analyzed the slip length by counting the number of slip events as a function of the sleep length. For all tips a maximum in the frequency of slip events was observed for a range of slip length l_{slip} = 0.256–0.3 nm (see Figs. 5(a)–5(c)); for comparison the interatomic distance of Au in its [110] crystallographic direction is $a_{[110]}$ = 288 pm.

The width of the slip distance distribution however significantly changed depending on the chemistry of the counter-bodies. In agreement with above observations the width of the slip-length distribution is narrowest for the Au-coated tip and increases in the order of the PtSi-coated and Pt-coated tips. In these later cases, the slip length distribution can be rationalized as a sharp maximum for the $a_{[110]}$ interatomic distance overlaid by a wider distribution of slip lengths. As shown in Fig. 6 the slip length distributions for all three counter-bodies were not significantly affected by the normal load, except at the highest applied load in this work F_n = 10 nN, at which wear was observed to set on and atomic

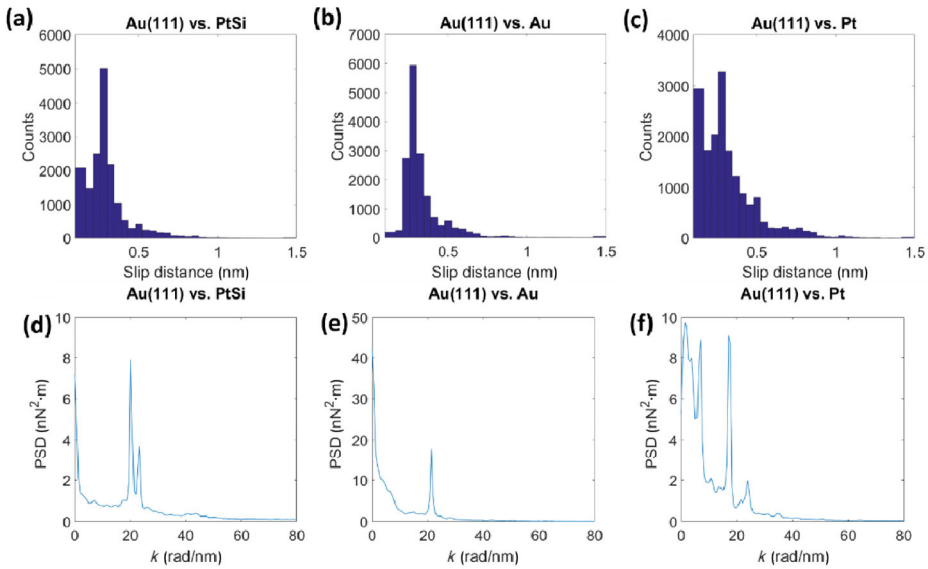

Fig. 5 (a–c) Slip-length distribution and (d–f) average one-dimensional power spectrum density functions calculated from FFM-images recorded on Au(111) with (a, d) a PtSi-coated tip, (b, e) a Au-coated tip, and (c, f) a Pt-coated tip.

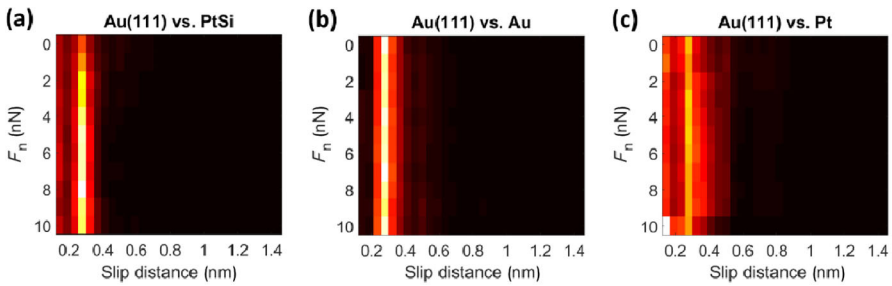

Fig. 6 Slip-length distribution on Au(111) as a function of the normal load with (a) a PtSi-coated tip, (b) a Au-coated tip, and (c) a Pt-coated tip.

stick-slip partially disappeared. In particular, at F_n = 10 nN the slip-length distribution corresponding to the Au(111)/Pt tribological couple exhibited a less prominent maximum for l_{slip} and a wider distribution of slip lengths on the overall.

In order to further characterize the degree of order at the interface between Au(111) and the different counter-bodies used in our friction experiments, we further approximated the averaged power spectrum density (PSD)-functions of the friction signals recorded at different loads. Figures 5(d)–5(f) show typical PSD-functions for the three different tips used on Au(111). The PSD-function corresponding to a typical friction measurement on Au(111) with a Au-coated tip shows a single peak at a wavenumber k = 21.36 rad/nm (see Fig. 5(e)). Neither the position nor the amplitude of this peak were found to change upon increasing load; except for F_n = 10 nN, in which case two slightly less prominent peaks were observed at k = 20.11 rad/nm and k = 22.62 rad/nm (see Fig. 7(b)). For the PtSi-coated tip a typical PSD-function shown in Fig. 5(d) exhibits two maxima at k = 20.11 rad/nm and k = 23.25 rad/nm. These two peaks were observed for a load ranging from 0 to 8 nN. At higher load values up to F_n = 10 nN, a single peak was observed at k = 21.36 rad/nm (see Fig. 7(a)). A power density spectrum corresponding to the Pt-coated tip sliding on Au(111) is shown in Fig. 5(f). There, three most prominent peaks are observed at k = 6.28 rad/nm, k = 16.96 rad/nm and k = 23.88 rad/nm. Further peaks can be further recognized in Fig. 7(c) at k = 10.05 rad/nm, k = 13.82 rad/nm, k = 34.56 rad/nm and k = 50.27 rad/nm, the intensities of which increase with the normal load.

The characteristic wavelength λ-values corresponding to the above wavenumbers are listed in Table 3. In the case of the PtSi- and Au-coated tips the characteristic wavelength λ_2 = 0.294 nm corresponds to the interatomic distance of Au in the [110] direction ($a_{[110]}$ = 288 pm). The small discrepancy arises from the numerical approximation of the PSD function. In Figs. 4(d), 6(a) and 6(b) the maximum in the PSD-functions are also found to split into two equidistant peaks with corresponding wavelength-values λ_3 = 0.277 nm and λ_1 = 0.312 nm, respectively. We attribute these peaks to the herringbone reconstruction of the Au(111) surface and the resulting different tilt angles of the fcc and hcp domains with respect to the unreconstructed surface [23]. For the Pt-coated tip three main characteristic wavelengths can be determined from Figs. 5(f) and 7(c): λ_1 = 1 nm, λ_2 = 0.37 nm, and λ_3 = 0.263 nm. The smaller of these values may correspond to the Pt–Pt interatomic distance. The metallic radius of Pt is given in the literature as 0.138 nm [24], which corresponds to the interatomic distance of pure Pt in the [110] crystallographic direction $a_{[110]}$ = 0.276 nm. The difference between this value and the one obtained from the PSD function may arise from the numerical approximation. Further the λ_2-value found for the

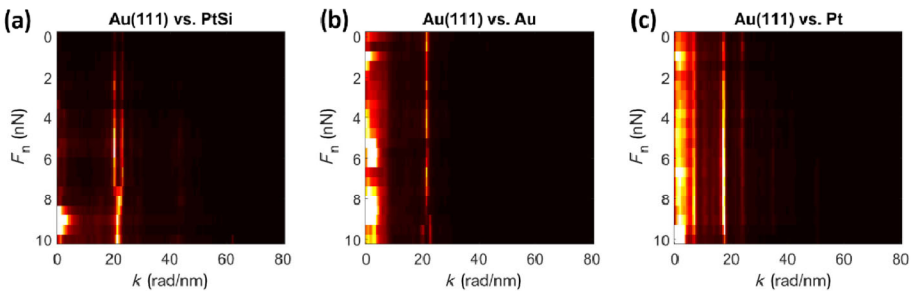

Fig. 7 Load dependence of the power spectrum density functions calculated from FFM measurements on Au(111) with (a) a PtSi-coated tip, (b) a Au-coated tip, and (c) a Pt-coated tip.

Table 3 Characteristic wavelength λ corresponding to the wavenumber k of the power density function maxima.

Counter body	k_1 (rad/nm)	k_2 (rad/nm)	k_3 (rad/nm)	λ_1 (nm)	λ_2 (nm)	λ_3 (nm)
PtSi	20.11	21.36	23.25	0.312	0.294	0.277
Au	20.11	21.36	22.62	0.312	0.294	0.277
Pt	6.28	16.96	23.88	1	0.37	0.263

Pt-coated tip matches literature values for the lattice parameters of Au-Pt intermediate phases such as Au_3Pt (cubic lattice; a = 0.392 nm), AuPt (tetragonal lattice; a = 0.392 nm and c = 0.39) or $AuPt_3$ (cubic lattice; a = 0.392 nm) [14].

To support these results we analyzed the Pt-coated tip used Au(111) with regard to its elemental chemistry by energy dissipative X-ray spectroscopy (EDS) inside a SEM. Figure 8(a) shows the energy spectrum recorded with an electron acceleration voltage of 10 kV on an area equivalent to the overlaid circle at the tip apex in Fig. 2(c). From this spectrum five elements were detected: C, O, Si, Pt and Au. Figures 8(b)–8(d) are magnifications of the spectrum in Fig. 8(a). As shown in Fig. 8(b) the most prominent EDS-peak was found at an energy value 0.277 keV that corresponds to the Kα-spectral line of carbon and is a result of contamination. Although Pt and Au have N-spectral lines at 0.251 keV and 0.258 keV, respectively, fitting this peak with the sum of three distinct Gaussian distributions did not yield a satisfactory deconvolution. This can be explained by the prominence of the carbon signal compared to the ones for Pt and Au. A second peak was detected at an energy value 0.525 keV that corresponds to the Kα-spectral line of oxygen (see Fig. 8(c)). In Fig. 8(d) three peaks can be distinguished. There, a first peak at an energy value 1.74 keV is associated to the Kα-spectral line of silicon, which is the basis material of the AFM-tip. A second peak is found to consist in the convolution of two Gaussian distributions: one associated to the Mα-spectral line of Pt at an energy value 2.05 keV that corresponds to the coating material of the tip and the other to the Mα-spectral line of Au at an energy value 2.123 keV, that is associated to transferred material from the Au(111) surface to the tip. The elemental peak areas were further used to evaluate the chemical concentration at the tip apex. Thereby, only the elemental peaks for Si, Pt, and Au were considered. We found X_{Si} = 71.3 at.%, X_{Pt} = 25.35 at.% and X_{Au} = 3.35 at.%. The volume probed by EDS reaches far below the tip surface, as indicated by the detection of Si. The Pt-coating thickness is given by the manufacturer to be ~100 nm. These two factors explain the larger concentrations of Si and Pt compared to the Au-concentration, since Au is expected to be localized at the tip surface. It is therefore expected that the Au/Pt-surface concentration ratio is significantly larger than 0.13 as calculated from the above concentration values. To obtain an accurate value of the chemical surface composition and structure of the tip surface, small area x-ray photoelectron spectroscopy and atom probe tomography should be used. The application of both methods remains however very challenging

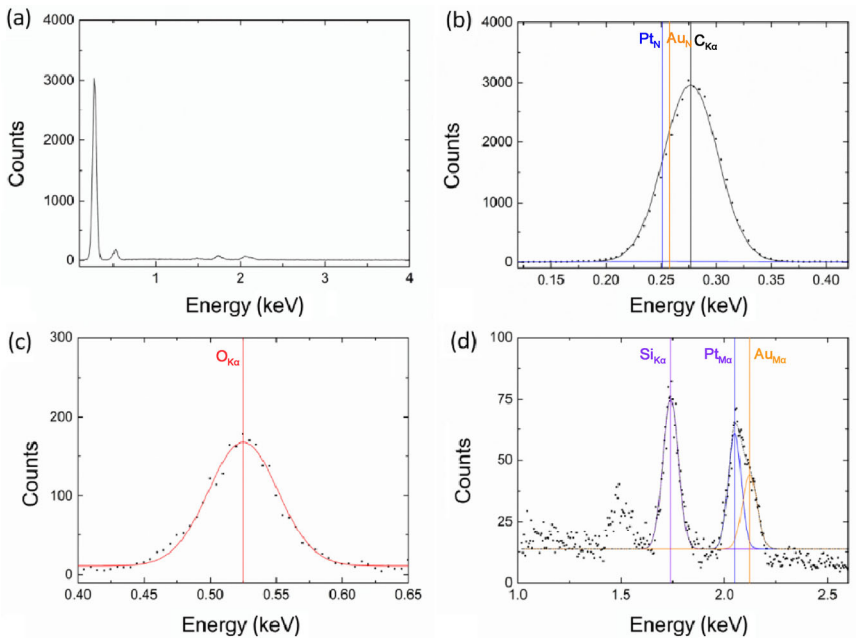

Fig. 8 Chemical EDS-analysis of a Pt-coated tip used for friction measurements on Au(111).

at this moment. To the best of the authors knowledge, none of these methods has been applied to determine the chemical composition or structure at the surface of an AFM tip. Alternatively, a combination of transmission electron microscopy (TEM) and electron energy loss spectroscopy could be applied to provide a lateral resolution than provided by EDS. However, the collected electron signal would in this case too have a contribution from the tip volume through which the primary electron would transmit.

5 Discussion

According to Bowden and Tabor, the friction force during relative sliding between metallic surfaces results from the formation of junctions at surface asperities and their shearing [1]. The formation of junctions can proceed by severe plastic deformation and cold welding. In such cases, the shear strength of a junction relates to its resistance to plastic deformation and shearing off the junction usually results in materials transfer from the softer to the harder asperity. The macroscopic sliding friction of metals has been extensively investigated by Rigney [25]. It has been reported that material transfer occurs for both miscible and immiscible tribological partners. In both cases, smearing of the softer metals onto the harder one has been observed. Also, Rabinowicz has suggested that during adhesive wear between metals the friction coefficient depends on their respective phase diagrams [2], i.e., metallurgical compatibility, with compatible metals having a high friction coefficient due to their work of adhesion. There, the work of adhesion $W_{ad} = c_m(\gamma_a + \gamma_b)$, where c_m is a compatibility factor between the metals *a* and *b* with the respective surface energies γ_a and γ_b. Based on the experimental determination of the work of adhesion between different metals and their respective surface energies, the values of c_m have been calculated to be 1 for identical metals and to decrease to 0.5 for compatible metals and to 0.2 for incompatible metals. Under unlubricated conditions, Rabinowicz reported the friction coefficient between metals subjected to adhesive wear to be 0.8 for identical metals and to decrease to 0.63 for compatible metals and to 0.35 for incompatible metals [2]. Following a similar scheme, Ando et al. measured the friction coefficient of various metallic couples and discussed their results based on the difference in atomic sizes of the involved elements [26]. The authors found that friction was largest for small atomic size differences between the tribological partners. This corresponds to the situation where the formation of substitutional solid solution is not impeded by strain energy.

Table 4 lists the values of surface energies for the investigated materials, for which the adhesion energy values were calculated using the c_m-values suggested by Rabinowicz. Thereby, Rabinowicz considered both Ag and Pt or Au and Pt to be compatible, while their respective equilibrium phase diagrams indicate almost no solubility at room temperature [14]. The Ag-Pt equilibrium phase diagram shows a peritectic decomposition of the liquid phase with a peritectic temperature of 2,139 K and a peritectic concentration

Table 4 Surface energy γ [2], calculated adhesion work per unit surface W_{ad}, atomic radius *r* [24], relative atomic difference $\Delta r/r$, and enthalpy of mixing. [†] Calculated surface energy value for PtSi from Ref. [29]; [‡] the c_m-values correspond to the values for the studied metallic pairs suggested in Ref. [2]; [*] the *r*-value given for PtSi corresponds to the half bond length between Pt and Si as reported in Ref. [30]; [◊] this value corresponds to the excess enthalpy of the equimolar Ag-Pt solid solution [14]; [+] the ΔH_{mix}-value between PtSi and Au or Ag is here assumed to be largely positive; [#] this value corresponds to the calculated excess free Gibbs energy of formation of solid Au−Pt alloys at 1,423 K reported in Ref. [14].

	Ag	Au	Pt	PtSi	Ag-Au	Ag-Pt	Ag-PtSi	Au-Au	Au-Pt	Au-PtSi
γ (J/m^2)	0.92	1.12	1.8	1.4[†]	—	—	—	—	—	—
c_m	—	—	—	—	0.8[‡]	0.8[‡]	0.2	1	0.8[‡]	0.2
W_{ad} (J/m^2)	—	—	—	—	1.63	2.17	0.46	2.24	2.33	0.5
r (pm)	144	144	138	103[*]	—	—	—	—	—	—
$\lvert\Delta r/r\rvert$ (%)	—	—	—	—	0	3.82	28.47	0	3.82	28.47
ΔH_{mix} (kJ/mol)	—	—	—	—	−4.5	6[◊]	∞[+]	0	6[#]	∞[+]

of X_{Pt} = 40.6 at.% and a phase mixture of Ag and Pt at room temperature. The preparation of Ag–Pt metastable solid solution has been reported in Ref. [27], where the authors used splat cooling to quench the homogeneous Ag–Pt liquid phase. In Ref. [28], Peng et al. have reported on the organometallic synthesis and stability of Ag–Pt nanoalloys, i.e., nanoparticles consisting in solid solutions within the miscibility gap of the Ag–Pt system. This may indicate a larger contribution of the entropy of mixing at surfaces than in the bulk. According to Ref. [14], the excess enthalpy of the equimolar Ag-Pt solid solution is 6 kJ/mol.

It is interesting to compare the values of the adhesion force and friction coefficient listed in Table 2 for the same metals combination as in Table 4. We observe a better correlation between the measured adhesion force and enthalpy of mixing or the relative atomic size difference than with the calculated energy of mixing based on the compatibility parameter. However, our results are insofar in contrast to earlier works by Rabinowicz or Ando et al. that in the present work metallic couples having a high adhesion exhibit a low friction coefficient and vice versa.

In Refs. [2, 26] the friction was measured at the macroscale, in which case the contact between metallic surfaces is known to consist of many asperities that undergo plastic deformation leading to the cold welding of junctions. In this configuration friction corresponds to the resistance of these junctions to be sheared. Ultimately, the shearing of junctions leads to their fracture and results in material transfer of the softer metal onto the harder. In our experiments the response of a single nanometer-scale metallic asperity sliding on metal was recorded in the wear-less regime as indicated by the occurrence of atomic stick-slip on the Au(111) surface (see Fig. 4). In Ref. [5], the authors investigated the sliding friction behavior of single crystalline metallic surfaces by AFM under UHV-conditions and by using a SiO_x tip as a single-asperity counter-body. There, the friction force was observed to vanish in the adhesive regime. Although in this regime almost no energy dissipation was observed, the lateral force signals were characterized by a clear atomic stick-slip modulation. At higher loads, i.e., in the regime of repulsive forces, wear was observed to set on: the periodicity of stick-slip was disrupted and significant friction was measured. In Ref. [6], Gosvami et al. investigated the ageing of single-asperity sliding contacts between an AFM-tip and an Au(111) surface at low temperature and under UHV conditions. There the authors also observed stable stick-slip with atomic periodicity. An interesting observation was that at low temperature friction increased with time and resulted in a distortion of the stick-slip behavior. Reinitializing the contact after pulling out the tip away from the surface resulted in a decrease of friction and the restoration of atomic stick-slip periodicity. These experimental results were further supported by molecular dynamics simulation of the growing process of gold junctions. The authors concluded that periodic stick-slip observed at room temperature is the result of a dynamic equilibrium of the contact that involves surface diffusional self-healing of microscopic wear damage. The results by Gosvami et al. are further in line with previous results by Merkle and Marks demonstrating the wetting of a sharp tungsten tip by a gold surface and subsequent formation and elongation of a neck upon pulling the tip away from the surface [31]. More recently, Cihan et al. pointed at the importance of chemical inertness of the tribological couple and the abesence of contamination at the sliding interface for superlubricity. In ambient conditions, the authors reported a $F_n^{2/3}$-dependence of the friction force on gold [8]. However, the friction force arising from sliding a gold nano-island deposited on graphite yielded similar friction force values as in UHV conditions [9].

Our experimental results indicate that a high adhesion force corresponds to high friction force values and to low shear strength values. For low adhesive contacts, the friction forces are found to significantly increase with the normal load and correspond to a larger shear strength value. Our measurements were all performed under same ambient conditions (T = 293 K and RH = 40%). For such conditions, it has been known that an adsorbed water layer at the interface between tip and sample surface can affect the adhesion force to a degree dependent on the hydrophilic character of the involved surfaces in the contact. Our results do not allow to exclude the role of water. However, all involved metal surface materials are hydrophilic in nature as indicated by the similar

adsorption energy of water onto them (see Ref. [32]). It thus appears reasonable to consider the contribution of adsorbed water to the adhesion force as a constant off-set value for all tribological couples investigated in this work that do not affect the relative differences reported here.

The relation between the friction forces, the shear strength and the adhesion force can be explained by the formation of a stable and load independent junction geometry in the case of miscible systems such as Ag-Au and Au(111)-Pt that is most probably assisted by wetting effects. For immiscible systems such as Ag-PtSi, Au(111)-PtSi and Ag-Pt the formation of the tip-sample junction is supposed to be mediated by plastic deformation, as inferred in Ref. [5]. The formation of a junction in the case of the Au(111)-Au system appears to be both affected by wetting and plastic deformation, giving raise to both high adhesion and shear strength.

Figures 4–7 show the differences in stick-slip characteristics during sliding friction measurements on Au(111) with different tips. With a PtSi-tip and an Au-tip, clear periodic stick-slip events were observed. There, the periodicity coincided with the interatomic distance between Au atoms in the [110]-direction. Also, in the case of the PtSi-tip a further modulation of the friction signal was observed that has been attributed in Ref. [23] to the Herringbone reconstruction of the Au(111) surface. In our statistical analysis, the presence of the Herringbone reconstruction resulted in a splitting of the PSD-peak, into two symmetrical peaks around the value corresponding to the interatomic distance of Au atoms in the [110] direction. With a Pt-tip however, we observed a clear disruption of the stick-slip periodicity. In Fig. 5(f) a broad peak at low k-values indicates the occurrence of a rather disordered structure. Although, a clear peak is observed at k = 16.96 rad/nm that may correspond to the lattice parameter of an Au-Pt intermediate phase. The formation of Au_3Pt or AuPt intermetallic phases has been reported in the case of alloyed nanoparticles and surfaces in Refs. [33, 34]. Although our results do not allow to determine the formation mechanisms for such an interfacial phase, our EDS-results indicate a significant amount of Au transferred to the surface of the Pt-coated tip and we propose that the formation of an interfacial phase could be assisted by mechanical mixing during the drag of a Pt-Au(111) junction.

6 Conclusions

Comparing the friction behavior of miscible and immiscible couples we find that in the first case friction is governed by adhesion and the shear strength has a low value. In the latter case of immiscible couples, adhesion is found to be low and the shear strength exhibits a large value. Statistical analysis of atomic stick-slip images recorded on an Au(111) surface with tips of different affinities with gold allows for a deeper understanding of our results. Expectedly, the periodicity of atomic stick-slip images corresponds to the interatomic distance of gold for immiscible counter-bodies. In contrast, for a reactive couple the periodicity of atomic stick-slip significantly differs from the gold interatomic distance and may correspond to structural length of an ordered phase at the tip-surface interface. These results provide new insights in the formation of interfacial alloys and their effects on metals friction. Furthermore, our findings shall serve as new guidelines for the selection of materials couples for micromechanical devices involving sliding contacts.

Acknowledgement

This work was supported by KoreaTech.

Electronic Supplementary Material: The Matlab software packages (script1.m, script2.m, and script3.m) are available in the online version of this article at https://doi.org/10.1007/s40544-017-0167-5.

References

[1] Bowden F P, Tabor D. *The Friction and Lubrication of Solids*. Oxford (UK): Oxford University Press, 1950.

[2] Rabinowicz E. *Friction and Wear of Metals, 2nd edition.* New York (USA): John Wiley & Sons Inc., 1995.

[3] Mahalic N P (Ed.). *Micromanufacturing and Nanotechnology*. Heidelberg (Germany): Springer, 2006.

[4] Kim S H, Asay D B, Dugger M T. Nanotribology and MEMS. *Nanotoday* **2**: 22–29 (2007)

[5] Gosvami N N, Filleter T, Egberts P, Bennewitz R. Microscopic friction studies on metal surfaces. *Tribol Lett* **39**: 19–24 (2010)

[6] Gosvami N N, Feldmann M, Peguiron J, Moseler M, Schirmeisen A, Bennewitz R. Ageing of a microscopic sliding gold contact at low temperatures. *Phys Rev Lett* **107**: 144303 (2011)

[7] Bennewitz R, Hausen F, Gosvami N N. Nanotribology of clean and modified gold surfaces. *J Mater Res* **28**: 1279–1288 (2013)

[8] Cihan E, Özogul A, Baykara M Z. Structure and nano-tribology of thermally deposited gold nanoparticles on graphite. *Appl Surf Sci* **354**: 429–436 (2015)

[9] Cihan E, Ipek S, Durgun E, Baykara M Z. Structural lubricity under ambient conditions. *Nat Comm* **7**: 12055 (2016)

[10] Caron A, Louzguine-Luzgin D V, Bennewitz R. Structure vs. chemistry: Friction and wear of Pt-based metallic surfaces. *ACS Appl Mater Interfaces* **5**: 11341–11347 (2013)

[11] Bennewitz R. Friction force microscopy. In *Fundamentals of Friction and Wear*. Gnecco E, Meyer E (Eds.). Heidelber (Germany): Springer, 2007.

[12] Colgan E G, Gambino J P, Hong Q Z. Formation and Stability of silicides on polycrystalline silicon. *Mat Sci Eng R* **16**: 43–96 (1996)

[13] Topor L, Keppla O J Z. Thermochemistry of the systems Pd-Si and Pt-Si at 1400 K. *Metallkd* **77**: 65–71 (1986)

[14] Madelung O (Ed.). *Landolt-Boernstein—Group IV Physical Chemistry Volume 5A.* Berlin, Heidelberg (Germany): Springer, 1991.

[15] Butt H-J, Jaschke M. Calculation of thermal noise in atomic force microscopy. *Nanotechnology* **6**: 1–7 (1995)

[16] Gnecco E, Bennewitz R, Pfeiffer O, Socoliuc A, Meyer E. Friction and wear on the atomic scale. In *Nanotribology and Nanomechanics: An Introduction*. Bhushan B (Ed.). Berlin, Heidelberg (Germany): Springer, 2005.

[17] In this work we used the version R2015b. Matlab is manufactured and distributed by MathWorks, U.S.A.

[18] Meyer E, Luethi R, Howald R, Bammerlin M, Guggisberg M, Guentherodt H-J. Site-specific friction force spectroscopy. *J Vac Sci Technol B* **14**: 1285–1288 (1996)

[19] Johnson K L. *Contact Mechanics*. Cambridge (U.K.): Cambridge University Press, 1985.

[20] Carpick R W, Ogletree D F, Salmeron M. Lateral stiffness: A new nanomechanical measurement for the determination of shear strengths with friction force microscopy. *Appl Phys Lett* **70**: 1548–1550 (1997)

[21] James A M, Lord M P. Macmillan's Chemical and Physical Data. London (U.K.): Macmillan, 1992.

[22] Koc H, Deligöz E, Mamedov A M. The elastic, electronic, and optical properties of PtSi and PtGe compounds. *Phil Mag* **91**: 3093–3107 (2011)

[23] Li Q, Dong Y, Martini A, Carpick R W. Atomic Friction modulation on the reconstructed Au(111) surface. *Tribol Lett* **43**: 369–378 (2011)

[24] Greenwood N N, Earnshaw A. *Chemistry of the Elements, 2nd Edition.* Oxford (U.K.): Elsevier, 1997.

[25] Rigney D A. Sliding wear of metals. *Ann Rev Mater Sci* **18**: 141−163 (1988)

[26] Ando Y, Tamura Y, Takahashi H, Hiratsuka K. Experimental studies on revealing a dominant factor in friction coefficient between different metals under low load conditions. *Tribol Lett* **47**: 43–49 (2012)

[27] Ebert H, Abart J, Voitlaender J. Metastable solid solutions in Ag-Pt alloys. *J Less-Common Metals* **91**: 89–96 (1983)

[28] Peng Z, Yang H. Ag-Pt Alloy nanoparticles with the compositions in the miscibility gap. *J Sol State Chem* **181**: 1546–1551 (2008)

[29] Bentmann H, Demkov A A, Gregory R, Zollner S. Electronic, optical, and surface properties of PtSi. Thin films. *Phys Rev B* **78**: 205302 (2008)

[30] Paul J B, Scherer J J, Collier C P, Sykally R J. Cavity ringdown laser absorption spectroscopy and time-of-flight mass spectroscopy of jet cooled platinum silicides. *J Chem Phys* **104**: 2782–2788 (1996)

[31] Merkle A P, Marks L D. Liquid-like tribology of gold studied by *in-situ* TEM. *Wear* **256**: 1864–1869 (2008)

[32] Hodgson A, Haq S. Water adsorption and the wetting of metal surfaces. *Surf Sci Rep* **64**: 281–451 (2009)

[33] Deng L, Hu W, Deng H, Xiao S. Surface segregation and structural features of bimetallic Au-Pt nanoparticles. *J Phys Chem C* **114**: 11026–11032 (2010)

[34] Bergbreiter A. Atomic structure, stability and formation of surface confined alloys. PhD-Thesis. University of Ulm, Faculty of Natural Sciences, 2011.

Arnaud CARON. He is a materials scientist with expertise in the multi-scale mechanical behavior of materials, surfaces and micro-components. Since 2015 Arnaud Caron is assistant professor in the School of Energy, Materials and Chemical Engineering at KoreaTech–Korea University of Technology and Education, Republic of Korea. Arnaud Caron obtained his engineering degree in materials science in 2004 from the University of Saarland, Germany and was awarded with the Schiebold Medal. In 2009 he earned his doctoral degree in materials science from the University of Saarland, Germany. From 2007 to 2015 Arnaud Caron worked as a research associate at the Institute of Micro- and Nanomaterials of the University of Ulm, Germany, the WPI-Advanced Institute of Materials Research, Japan and the Leibniz–Institute for New Materials, Germany.

Hui Eun KO. She received her bachelor degree in material science and engineering in 2016 from KoreaTech—Korea University of Technology and Education, Cheonan, Republic of Korea. Since then, she has been studying for her master degree in material science and engineering at KoreaTech. Her research interests include nano-tribology and mechanical properties of metals and metallic glasses.